

Submitted to Biointerphases

Computer Simulations of the interaction between SARS-CoV-2 spike glycoprotein and different surfaces

David C. Malaspina¹ and Jordi Faraudo^{1, a)}

Institut de Ciència de Materials de Barcelona (ICMAB-CSIC), Campus de la UAB, 08193 Bellaterra, Barcelona, Spain

(Dated: 31 July 2020)

A prominent feature of coronaviruses is the presence of a large glycoprotein spike protruding from a lipidic membrane. This glycoprotein spike determines the interaction of coronaviruses with the environment and the host. In this paper, we perform all atomic Molecular Dynamics simulations of the interaction between the SARS-CoV-2 trimeric glycoprotein spike and surfaces of materials. We considered a material with high hydrogen bonding capacity (cellulose) and a material capable of strong hydrophobic interactions (graphite). Initially, the spike adsorbs to both surfaces through essentially the same residues belonging to the receptor binding subunit of its three monomers. Adsorption onto cellulose stabilizes in this configuration, with the help of a large number of hydrogen bonds developed between cellulose and the three receptor binding domains (RBD) of the glycoprotein spike. In the case of adsorption onto graphite, the initial adsorption configuration is not stable and the surface induces a substantial deformation of the glycoprotein spike with a large number of adsorbed residues not pertaining to the binding subunits of the spike monomers.

The following article has been submitted to the journal Biointerphases. After it is published, it will be found at <https://avs.scitation.org/journal/bip>

I. INTRODUCTION

The novel coronavirus SARS-CoV-2 (Figure 1a) emerged in December 2019 as a human pathogen⁵ that causes the COVID-19 disease outbreak that rapidly spread worldwide⁶. This virus belongs to the family of *Coronaviridae* and it is the third documented spillover of an animal coronavirus to humans in only two decades that has resulted in a major epidemic⁵.

Coronaviruses are enveloped, single-stranded RNA viruses, with the typical structure shown in Figure 1b. The virus envelope contains lipids and several proteins. These are the so-called envelope (E) and membrane (M) proteins, which play essential roles during virion assembly⁷ and the spike glycoprotein (S) which is responsible for the interaction of a coronavirus particle with a host cell receptor (the ACE2 human receptor, in the case of SARS-CoV-2⁸). The large protruding glycoprotein spikes on the envelope of coronaviruses give a characteristic appearance to this virus family, and give them their name (from "corona", which is Latin for "crown").

In an unprecedented effort, the scientific community has been able to rapidly identify not only the nature of the pathogen causing the COVID-19 disease but also most details of its molecular structure with atomistic resolution. For example the identification and full characterization of the virus⁹ was available in February 2020 and the atomistic structure of the spike glycoprotein, shown in Figures 1c,d, was published³ as early as in March 2020. At the time of writing, the Protein Data Bank¹⁰ hosts about ~ 300 structures related to the SARS-CoV-2 virus.

This wealth of experimental data has been also augmented with structures obtained from modelling techniques and molecular dynamics trajectories. Some of these studies consider the modelling of structural features which cannot be resolved experimentally in enough detail¹¹. Other studies consider aspects with direct biomedical implications: investigations of the molecular mechanisms related to the virus infection such as the binding of the virus spike with human receptors^{12,13}, identification of targets for vaccine development¹⁴ and molecular studies related to drug development^{15–17}. The exceptionally of the situation also lead to most of the computational groups working in this question to share the structures generated by their models and even full molecular dynamics trajectories, which are being deposited in public repositories such as the COVID-19 Molecular Structure and Therapeutics Hub¹⁸.

Our aim in this work is to contribute to these computational efforts by considering an important aspect not previously considered in simulation studies, namely the question of the interaction of the SARS-CoV-2 virus with surfaces of materials.

There is substantial evidence that surfaces of materials contaminated by viruses (called fomites in the medical nomenclature) play an important role in human-to-human transmission of many respiratory diseases of viral origin^{19–22}, including the particular case of SARS-CoV-2²³.

Many respiratory viruses are believed to spread from infected people through infected secretions such as saliva or their respiratory droplets, which are expelled when an infected person coughs, sneezes, talks or sings²⁴. These respiratory droplets from infected individuals can land on objects, creating fomites (contaminated surfaces)²³. A recent review of experimental and observational evidence indicates that coronaviruses deposited onto surfaces are able to remain infectious from 2 hours up to 9 days²², depending on the surface material and thermodynamic conditions such as humidity and temperature. In the case of SARS-CoV-1 and SARS-CoV-2, evidences from different groups²³ indicate that viable virus could be detected up to 4 hours on copper, up to 24 hours on cardboard and up to 2-3 days on plastic and stainless steel. This

^{a)}Electronic mail: jfaraudo@icmab.es

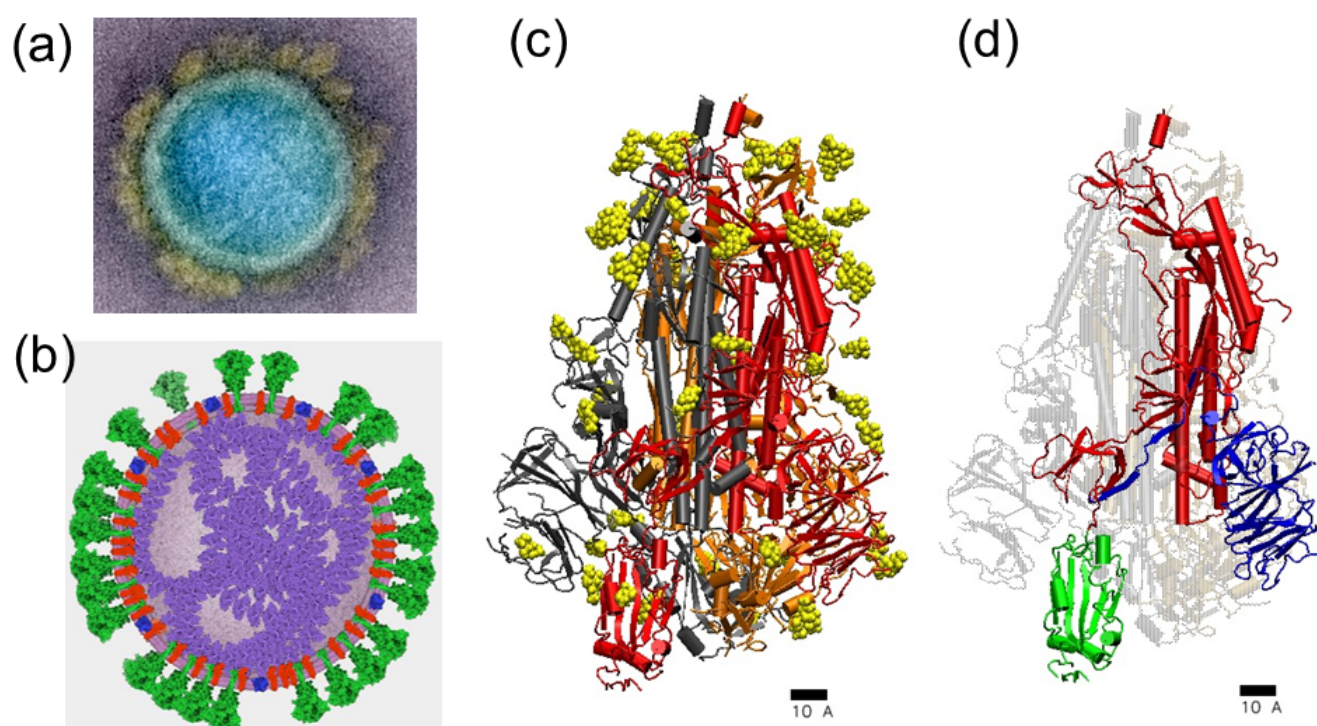


FIG. 1. (a) Electron microscopy image of a typical SARS-CoV-2 coronavirus particle, freely distributed by the NIAID's Rocky Mountain Laboratories (NIAID-RML)¹, colored to emphasize the virus structure. The spikes protruding from the virus envelope (in yellow color) are clearly visible. Typical diameter ranges from 80 nm to 120 nm. (b) General scheme of a coronavirus indicating their main structural features. We show the nucleocapsid (purple) that packages the viral RNA and the viral envelope. The major ingredients of the envelope are lipids (pink), envelope protein E (in blue), membrane protein M (in red) and the protruding spike glycoproteins (in green). The scheme was made by the authors using CellPAINT². (c) and (d) Snapshots of the atomistic structure of the SARS-CoV-2 trimeric glycoprotein spike available at the Protein Data Bank (PDB:6VSB). The scale corresponds to 1 nm. In (c) the protein is shown in cartoon representation with different colors for each monomer (grey, orange and red). The spike glycosylation is shown in yellow using Van der Waals representation. In (d) the structure of one of the monomers is emphasized. It has a membrane-fusion subunit S2 (in red) and a receptor-binding subunit S1 which has two independent domains (the receptor-binding domain RBD shown in green and the N-terminal domain NTD shown in blue). In this snapshot, the spike was in the prefusion conformation and the RBD shown in green was in its receptor-accessible state (the so-called "up" conformation)³. The snapshots were created using VMD⁴.

persistence of viable virus onto surfaces is the reason for recommendations of health authorities worldwide on continually disinfecting and cleaning surfaces that are frequently touched.

At the present time, there is a lack of fundamental understanding of interactions between coronavirus and surfaces at the physico-chemical level. We think that such a fundamental knowledge could be very useful in the design and interpretation of experiments involving coronavirus on surfaces and even contribute in the future to the rational design of disinfection measures.

Of course, the modelling of virus-surface interactions is a complex problem with multiple aspects to be considered. In the case of nonenveloped virus (such as bacteriophages for example), detailed studies show that the dominant interactions between virus and surfaces are electrostatic interactions and solvation interactions related to the hydrophobic or hydrophilic nature of the surface^{25,26}. Porosity and nanostructure of the surfaces at scales of the order of the virus size also have an impact²⁶.

In the case of coronavirus, it seems clear that the presence of the spike coverage in the virus envelope will play an important role in the virus-surface interaction. The spike is not only the most external feature of a coronavirus (see Figure 1) but also a protein which has interaction with other molecules as its main function. Given the fact that the molecular structure and atomistic coordinates of the SARS-CoV-2 virus spike are known³, a timely question is to consider the interaction between the spike and surfaces of materials. Starting from the available structure, we perform here atomistic Molecular Dynamics simulations of the SARS-CoV-2 virus spike and surfaces of materials in presence of hydration.

Given the relevance of the hydrophobic or hydrophilic character of the materials in virus-surface interactions, we will consider here two materials with very different characteristics: cellulose and graphite. Both materials are widely employed in adsorbents and filters. Cellulose is a material which is simultaneously hydrophilic and lipophilic since due to its molecular structure²⁷ both hydrogen bonding and the hydrophobic effect

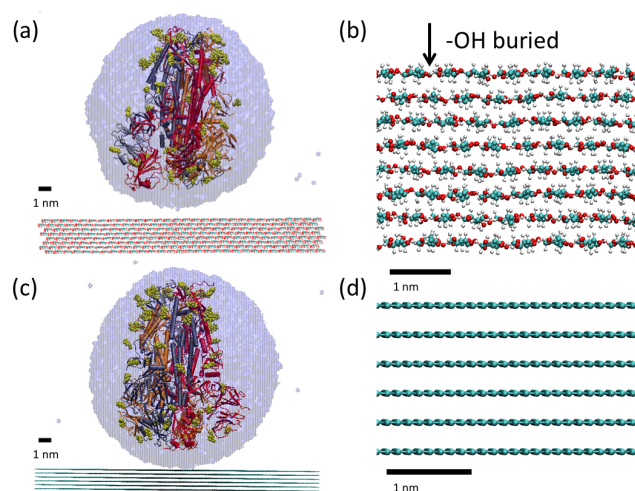


FIG. 2. a) Initial configuration for the simulation of the adsorption of a hydrated SARS-CoV-2 spike glycoprotein onto a cellulose surface. The protein is represented as in Figure 1c with its secondary structure with different colors for each monomer of the trimeric protein (red, grey and orange) and the glycosylation in yellow. The solvation sphere is also indicated (transparent blue). b) Detail (side view) of the cellulose surface. Buried -OH groups involved in cellulose-cellulose hydrogen bonds are indicated. c) Initial configuration for the simulation of hydrated SARS-CoV-2 spike glycoprotein on graphite surface. Color representation is the same as in a). d) Detail (side view) of the graphite surface.

play an essential role. In the case of graphite, its surface is strongly lipophilic and mildly hydrophilic²⁸, unable to pursue hydrogen bonds and prone to strong hydrophobic interactions.

Up to the best of our knowledge, this is the first study involving the interaction of the SARS-CoV-2 virus external elements with materials. The results may be also relevant for other coronavirus, since all of them share very similar spike glycoproteins.

II. SIMULATION RESULTS

A. Adsorption onto cellulose and graphite

We have performed all-atomic Molecular Dynamics (MD) simulations of a solvated glycoprotein spike near a cellulose and a graphite surface, as shown in Figure 2. As seen in this figure, we have considered the spike inserted inside a large pre-equilibrated water droplet ($\sim 6 \times 10^4$ water molecules). The reason for the inclusion of water in the simulation is that it is known that envelope virus (such as SARS-CoV-2) are transferred to surfaces in hydrated conditions (as discussed in the Introduction) and it is also known that the virus needs to be solvated in order to remain viable. The droplet also contains Na^+ counterions, neutralizing the charge ($-23e$) of the spike (both surfaces are neutral). Full technical details of the models employed and the protocols of the simulations are given in section IV Methods. The process of spike adsorption onto both surfaces is shown in the video provided in the support-

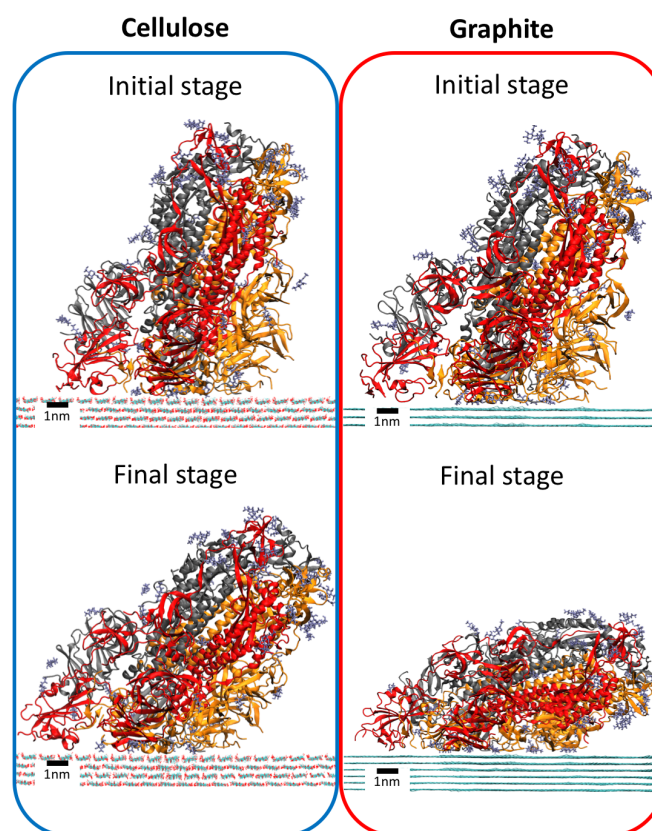


FIG. 3. Representative snapshots of SARS-CoV-2 spike glycoprotein during the first and final adsorption stage onto cellulose (left) and graphite (right) surfaces. The initial and final adsorption stage correspond to the time intervals indicated in section IV. Methods. Water molecules were not shown for simplicity. The glycoprotein is shown with cartoon representation and glycans are shown in licorice representation. Each monomer of the trimeric glycoprotein is shown with a different color with the same color code as in Figure 2. The surface is shown with line representation.

ing information and it is illustrated by the snapshots shown in Figure 3. The time evolution of the different quantities characterizing the adsorption process is shown in Figure 4.

The simulation results can be briefly summarized as follows. Initially, the spike adsorbs to both surfaces in a similar way (Figure 3), through contact of the receptor binding subunits of the spike with the surface. In the case of cellulose, this configuration is stable and the spike remains essentially in this configuration during all the simulation. In the case of adsorption onto graphite, the initial adsorption configuration is not stable and the surface induces a substantial deformation of the glycoprotein spike.

In order to discuss the results in more detail, it is useful to divide the adsorption process into two different stages, an initial stage corresponding to the contact of the spike with the surface and a final stage reached after structural changes of the spike over the surface.

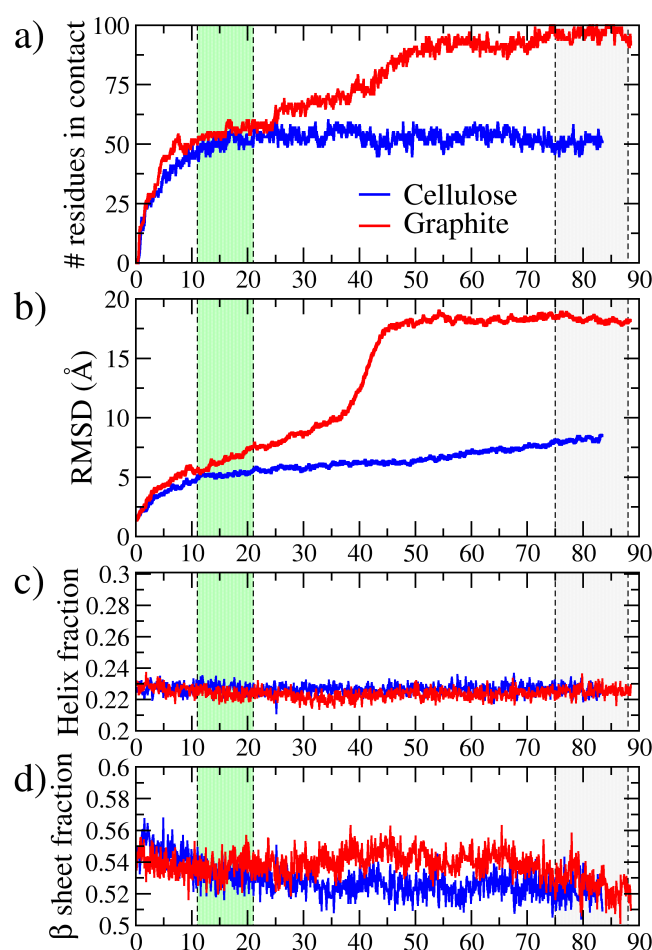


FIG. 4. Time evolution of physical quantities in the MD simulations of SARS-CoV-2 spike glycoprotein adsorption onto surfaces. (a) Number of residues in contact with each surface as a function of time. (b) RMSD as function of time. (c) Fraction of helix structures in the glycoprotein as function of time. (d) Fraction of beta sheet structures in the glycoprotein as a function of time. Blue lines correspond to the adsorption on the cellulose surface, while red lines correspond to adsorption on the graphite surface. Yellow and grey areas indicate the approximate location of the initial and final adsorption stage time intervals used in the calculations (see the section IV.Methods for the precise definition).

1. Initial adsorption stage

Full contact between the glycoprotein and the surfaces is established after $t \sim 10$ ns of simulation in both cases, as indicated by the stabilization of the number of aminoacids in contact with the surface seen in Figure 4a. The number of aminoacids in contact with the surface remains relatively stable for both surfaces (i.e. without abrupt changes) up to $t \sim 20$ ns, as seen in Figure 4a. We will consider this time interval (with about ~ 60 aminoacids of the spike in direct contact with the surfaces) as the initial adsorption stage, as highlighted in Figure 4. Illustrative snapshots of this stage are

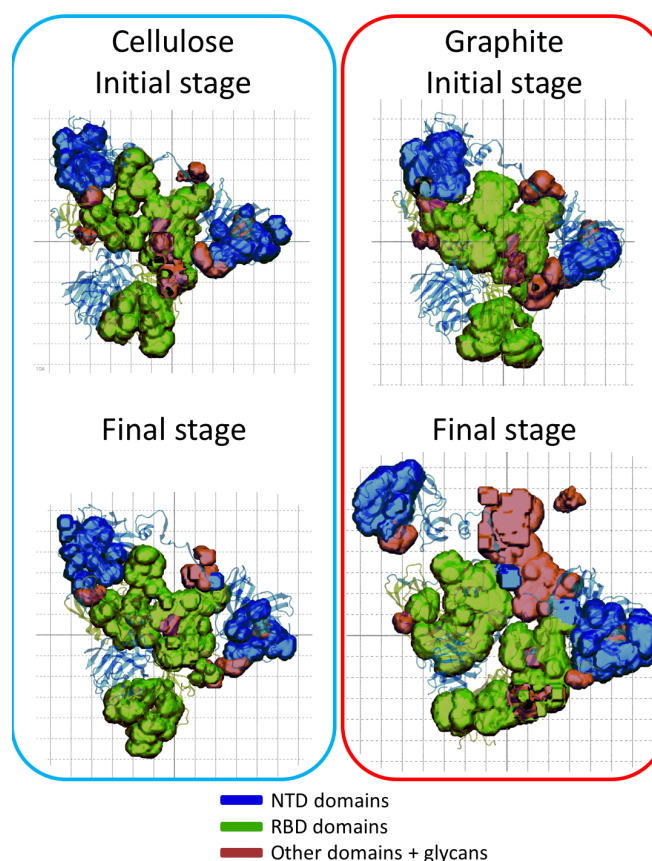


FIG. 5. 2-D volumetric map of the residues in contact with cellulose (left panels) and graphite (right panels) surfaces during the initial and final stage of adsorption (see section IV.Methods for details). The background grid spacing correspond to 1 nm. Color representation correspond to RBD domain (green), NTD domain (blue) and S2 domain + glycans (red). On top of the volumetric map is the structure of NTD and RBD in transparent cartoon representation.

shown in the top panels of Figure 3.

After adsorption ($t \sim 10$ ns), the RMSD between the adsorbed spike structure in absence of a surface and the adsorbed structure is ~ 5 Å for both surfaces (Figure 4b), indicating a small structural change during adsorption. In the case of adsorption onto cellulose, the RMSD remains constant during the initial adsorption stage but it steadily increases with time in the case of graphite. This can be considered as an indication that this adsorbed configuration of the spike onto graphite is not stable, as we will see.

Comparison of the snapshots in Figure 3 and the structure shown in Figure 2d suggests that this initial adsorption of the spike at the surfaces is made through contact between the surfaces and the subunit S1 of each monomer of the spike. This is confirmed by a detailed description of the contact region between the spike and the surface, as shown by the contacts map in Figure 5. As seen in this figure, in both cases (cellulose and graphite), the adsorption involves three RBD and two NTD domains of the receptor-binding subunit S1. In this initial stage, the spike has a similar distribution of contacts with both

surfaces although the distribution is more compact in the case of the graphite surface. Therefore, all three monomers are involved in the adsorption process, although in one monomer only the RBD domain is involved and in two monomers both the RBD and NTD domains of the S1 unit are involved. There is only slight contact between the surfaces and glycans or with the S2 subunit of the monomers.

2. Final adsorption stage

After a similar initial adsorption process, the subsequent evolution reflects (Figures 4a,b) the substantial differences between adsorption onto cellulose and graphite. In the case of the graphite surface, both the number of residues in contact with the surface and the RMSD show substantial evolution with time including abrupt changes (for example at $t \sim 40$ ns) whereas it shows only minor time evolution in the case of the cellulose surface. At long times ($t \sim 75$ ns), the spike adsorption onto graphite stabilizes, so we can define a final stage, as indicated in Figure 4, to compare the obtained structures for both surfaces. The most remarkable feature of the final stage is the striking deformation and curvature of the spike towards the graphite surface seen in Figure 3. This deformation is reflected in the large number of contacts of the spike with the graphite surface, which is near 100 residues in contact, as seen in Figure 4a. This deformation of the spike over the graphite surface involve structural changes captured by the time evolution of the RMSD (Figure 4b). The RMSD stabilizes at ~ 18 Å at the final stage, which implies a substantial structural change induced by graphite.

In the case of the cellulose surface, the number of residues of the glycoprotein in contact with the surface remains approximately constant (~ 50) between the initial and final adsorption stages. The RMSD remains at ~ 5 Å up to simulation times of $t \sim 50$ ns, and after that it increases slowly reaching ~ 8 Å. This change in RMSD corresponds to a slight deformation of the protein to increase its contact with the surface accompanied by a slight change of the orientation of the main axis towards the cellulose surface (see snapshot in Figure 3).

Figure 5 also shows substantial differences between the surface of contact between the spike and cellulose or graphite, as should be expected from Figure 3. The contacts between the spike and cellulose changed only slightly from the initial to the final stage whereas in the case of graphite the region of contact increased substantially, due to the deformation of the spike discussed above. Figure 5 also shows that in the case of graphite the adsorption involves not only the receptor-binding subunit S1 but also a substantial contact with the membrane-fusion subunit S2. Therefore, the substantial deformation of the spike observed in Figure 3 involves the adsorption of the membrane-fusion subunit S2 at the graphite surface.

Interestingly, neither the adsorption to graphite or cellulose induce changes in the secondary structure of the spike. According to Figures 4b,c there is no significant change in the secondary structure of the spike due to adsorption over surfaces since the percentage of α -helix (Figure 4c) and β sheets (Figure 4d) structures in the spike remain almost constant.

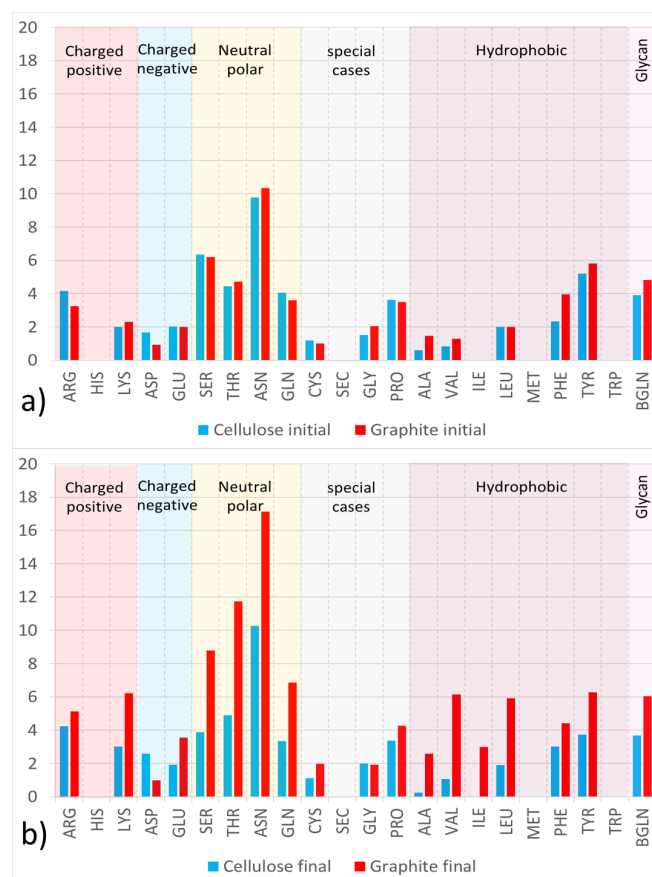


FIG. 6. Average number of spike aminoacids (3-letter code) in contact with cellulose (blue) or graphite (red) during (a) the initial stage of adsorption and (b) the final stage of adsorption (see section IV. Methods for details of the calculation). Each aminoacid is also classified into charged (positive or negative), neutral polar, hydrophobic or special cases. Glycans of the spike protein are also included.

This could be related to the fact that the spike is known to be rather flexible. In fact, it has been suggested²⁹ that the mechanism of binding of the spike of coronaviruses to diverse host cell receptors is based on the flexibility of the spike.

Before entering into a more detailed analysis of the spike-surface interactions, we would like to add a comment about the ions present in the simulation. As we mentioned before, the simulation also contains Na^+ counterions to neutralize the spike charge. The ions are observed to be mostly condensed at the spike, without being involved in the adsorption process. It is likely that the reason for this observation is that both surfaces are neutral and the spike is strongly charged.

B. Detailed analysis of protein-surface contacts

In order to obtain a deeper understanding of the adsorption results described in the previous subsection, we have performed a more detailed study of the particular aminoacids involved in the protein-surface interaction. In Figure 6, we show

the number of spike aminoacids in contact with cellulose or graphite, classified by aminoacid type, for both the initial and final adsorption stage.

In the initial stage (Figure 6a), we obtain a very similar distribution of residues of the spike in contact with both cellulose and graphite. The only difference is a slight tendency of graphite to favour more contacts with hydrophobic residues. In both cases, there is a substantial contribution from neutral polar aminoacids with $\sim 24 - 25$ contacts ($\sim 42-44\%$ of contacts), being ASN (Asparagine) with an average of about ~ 10 contacts ($\sim 17.5\%$ of the total) the most abundant residue in contact with the surface.

Overall, our results in Figures 5 and 6 imply that in the initial adsorption stage, the nature of the surface plays a minor role. In both cases, the spike is able to adsorb to both surfaces through essentially the same aminoacids located in the receptor-binding subunits S1 of the trimeric spike. However, it is possible that the magnitude of the interaction should be different for the different surfaces, given their different character regarding hydrogen bonding and hydrophobic interactions.

In order to compare the magnitude of the spike-surface interactions for both cases, we have performed additional simulations using the steering molecular dynamics technique. In these simulations, the spike is pulled from the surface at constant velocity and the required detachment force is monitored. Our results (reported in Appendix A), indicate that the detachment forces are very similar for both surfaces at the initial adsorption stage. For the faster detachment velocity (5nm/ns) the detachment force in both surfaces is approximately similar, being ~ 8100 pN for cellulose surface and ~ 8500 pN for the graphite surface. As we reduce the detachment velocity the difference in the maximum force between graphite and cellulose becomes more important, with graphite requiring a larger force to detach the glycoprotein from the surface. At the lower detachment velocity (1 nm/ns) the maximum force for cellulose surface is ~ 4900 pN and ~ 6200 pN for the graphite surface. This higher detachment force for the graphite surface could be related to the density of contacts as shown in Figure 5 at the initial adsorption stage. As seen in that figure, the graphite tends to form a more dense contact surface with the spike glycoprotein, which may require a larger force to detach from the surface.

The results for the analysis of the aminoacids involved in the protein-surface interaction during the final stage (Figure 6b) reflect the different evolution for the adsorption of the spike on cellulose or on graphite, in line with the results discussed in the previous subsection. In the case of graphite, the differences between the initial stage and the final stage in Figure 6 are obviously due to the deformation of the spike after adsorption described in the previous subsection. The total number of contacts of the spike with graphite increased from an average of ~ 59.2 contacts in the initial stage to ~ 102.8 in the final stage.

Again, the most abundant residue in contact with the graphite surface is ASN (asparagine) with an average of about ~ 17 contacts corresponding to a prominent peak in Figure 6b. This result is consistent with previous simulations that indicated a strong affinity of asparagine with carbon aromatic

rings³⁰. The final stage of adsorption at the graphite surface is dominated by contacts with asparagine, threonine, serine and glutamine neutral polar aminoacids but there is also a substantial number of contacts with hydrophobic aminoacids such as tyrosine, valine or leucine and with the glycans covering the lateral regions of the spike.

In the case of cellulose, the number of contacts remains nearly (only a very slight decrease in the total number of contacts, from a total of 55.6 in the initial stage to 54.2 in the final stage). Comparison between Figure 6a and Figure 6b shows very minor changes. In the final stage there are slightly more contacts with charged aminoacids and less contacts with hydrophobic aminoacids than those obtained in the initial stage. Therefore, the small changes observed in the previous subsection (both in the RMSD and the map of contacts, Figures 4b and 5) can be attributed to a rearrangement of the protein at the surface to increase interactions with hydrophilic aminoacids and reduce the contacts with hydrophobic aminoacids, without significantly changing the number of contacts. In any case, Figure 6 shows a wide variety of residues with different chemical affinity in contact with cellulose. Again the peak in the case of asparagine is the most noticeable feature for the case of cellulose in Figure 6b, with ~ 10 contacts (which corresponds to $\sim 19\%$ of contacts).

C. Detailed analysis of protein-cellulose hydrogen bonds

Overall, our results indicate that in the case of cellulose the spike is immobilized after adsorption, experiencing only minor changes during the adsorption process. This effect could be due to some sort of stabilizing interaction, that anchors the aminoacids of the receptor binding domain (RBD) after touching the surface.

Since the surface of cellulose has a large hydrogen bonding ability, this interaction could be responsible for the observed stabilization. In order to check this possibility, we have analyzed in detail the presence of hydrogen bonds between the spike and the cellulose surface (Figure 7). In Figure 7a, we show the number of direct hydrogen bonds between the spike and the cellulose surface. Similar to what is observed in Figures 4a and 4b with the number of contacts and the RMSD, the number of hydrogen bonds stabilizes after ~ 10 ns of simulation time and fluctuates around an average of ~ 18 hydrogen bonds total during the rest of the simulation. Further identification of these hydrogen bonds reveals that they are mostly located on the RBD domain of the glycoprotein, constituting almost $\sim 75\%$ of the total hydrogen bonds.

In Figure 7b, we report the number of hydrogen bonds for each aminoacid type together with the number of aminoacid-spike contacts. In the case of the neutral polar asparagine and serine, a significant number of the aminoacid-cellulose contacts involve hydrogen bonding. It is also interesting to note a significant number of hydrogen bonds with cellulose from the aminoacids of hydrophobic character leucine (LEU) and tyrosine (TYR) that have also the possibility of hydrogen bonding. Probably the amphiphilic character of cellulose²⁷ tends to enhance the interaction with these aminoacids.

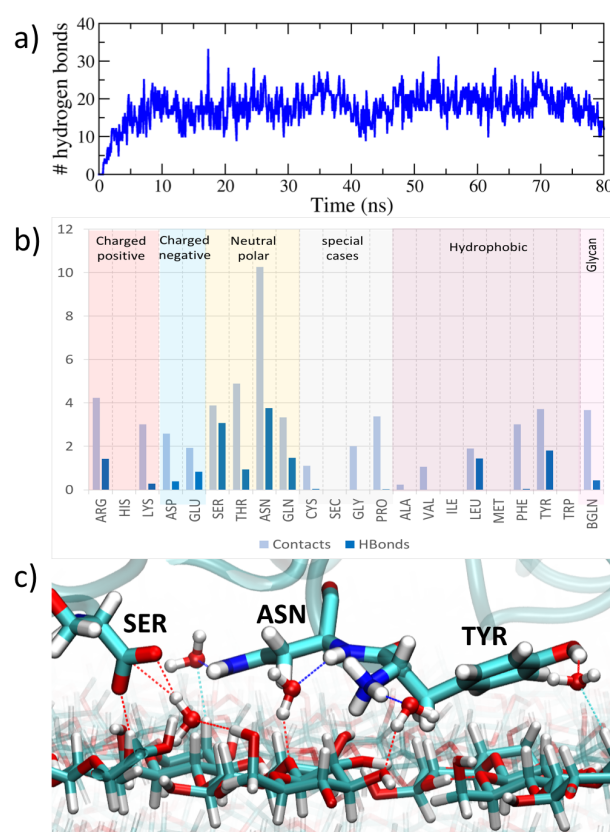


FIG. 7. Hydrogen bonds analysis. a) Time evolution of the number of hydrogen bonds between the spike and cellulose. b) Comparison of the distribution of contacts and hydrogen bonds by residues during the final stage of adsorption. c) Simulation snapshot ($t = 45$ ns) with a detail of some spike residues sharing hydrogen bonds with solvation water and cellulose). Highlighted spike residues are SER:443:B, ASN:450:B and TYR:449:B. The dotted lines indicate hydrogen bonds. Both cellulose and aminoacids are shown in licorice representation with CPK colors.

Hydrogen bonding between the spike and cellulose is more complex than simply due to direct cellulose-spike hydrogen bonds. A closer look to the formation of hydrogen bonds between the spike and cellulose reveals the existence of hydration water molecules that share hydrogen bonds with cellulose and aminoacids. In Figure 7c we can observe that three of the aminoacids with larger contributions in the number of hydrogen bonds in Figure 7b (ASN, SER and TYR) also form bridging hydrogen bonds with surrounding water, which makes hydrogen bonds with both the aminoacid and the cellulose surface.

Overall, this complex hydrogen bond network mainly located at the interface of the RBD domain tends to stabilize the spike glycoprotein on the cellulose surface and is possibly responsible for the differences in deformation observed between cellulose and graphite surfaces observed in Figure 3.

III. CONCLUSIONS

In this work we presented molecular dynamics simulation of the SARS-CoV-2 spike glycoprotein interacting with two different surfaces: cellulose and graphite. The choice of these surfaces was made in order to compare two different materials with very different properties. Cellulose is a complex molecular material with amphiphilic properties and a high quantity of hydrogen bonds donors and receptors. Previous works (see for example ref²⁷ and references therein) demonstrated the capacity of cellulose to bind proteins by both hydrogen bonding and hydrophobic interactions. On the contrary, graphite is a crystalline hydrophobic material with no hydrogen bond capability. It is also known to be able to bind peptides and proteins via hydrophobic interactions (see for example³⁰ or the discussion in Ref³¹).

Our simulation results can be summarized as follows:

Initially, the spike adsorbs to both surfaces through essentially the same residues belonging to the receptor binding subunit of its three monomers (in particular, involving all three receptor-binding domains (RBD) and two N-terminal domain (NTD)). From this point the adsorption on each surface dramatically differs.

Adsorption onto cellulose stabilizes in the initial adsorption configuration with the help of a large number of hydrogen bonds developed between cellulose and the three receptor binding domains (RBD) of the glycoprotein spike. This adsorbed configuration also includes shared hydration water between the spike and cellulose. In the case of adsorption onto graphite, the initial adsorption configuration is not stable and the surface induces a substantial deformation of the glycoprotein spike with a large number of adsorbed residues not pertaining to the binding subunits of the spike monomers.

Our results have interesting implications. First of all, let us note that the results are in line with previous results of other proteins in these surfaces that indicate that cellulose tends to adsorb proteins in stable configurations without structural changes²⁷ whereas the interaction with graphite induce substantial structural effects on adsorbed proteins³¹.

Concerning the possible practical implications of these results, obviously we need to remark that the present study is a simplification, since it ignores important effects such as the process of approach of the full virus to the surface, which is dominated by long range forces. Nonetheless, this represents the final stage of the adhesion of a virus with a surface, in which the most external element (the spike) interacts with the surface and it provides a reasonable approximation to the affinity between the virus particle and a given surface. With all these precautions in mind, we can say that our results suggest that interactions with cellulose will tend to maintain the integrity of the hydrated SARS-CoV-2 virus spike. Also, interactions with graphite deform the spike and may potentially help to inactivate the infectious potential of the spike glycoproteins interacting with the surface. As a recommendation for future experimental investigations, it will be of great interest to investigate the viability of the virus over carbon surfaces, in particular given the importance of these materials for filtration applications.

IV. METHODS

A. Simulation models and forcefields

All Molecular dynamics (MD) simulations reported in this paper were performed using NAMD 2.13 software³². The preparation of the simulation models and most of the analysis were made using Visual Molecular Dynamics (VMD) software⁴. The force field employed in the simulations is the CHARMM36 force field which includes parametrization of carbohydrate derivatives, polysaccharides and carbohydrate-Protein interactions³³. This forcefield is therefore appropriate for describing both the spike glycoprotein and all materials considered in the paper. The water model used in our simulations was the TIP3P model included in CHARMM36.

The atomic coordinates for the SARS-CoV-2 spike glycoprotein structure were obtained from a cryo-EM structure³ solved at 3.46 Å average resolution (PDB ID: 6VSB). This structure contains S1 and S2 spike subunits (with one RBD domain in "up" conformation) and a glycosylation pattern characterized by N-Acetyl-D-Glucosamine (NAG) residues, as shown in Figures 2c and 2d. The only modification made to this initial structure was the addition with VMD of missing hydrogen atoms and connecting links between the protein aminoacids and the NAG residues. The obtained structure contains 46,708 atoms and its total charge (assuming pH 7) is -23e.

It should be noted that the glycosylation pattern present in this structure only includes glycans in close proximity to the protein due to lack of further information on the resolved structure of the spike. We are aware of ongoing work on the development of more accurate models of the spike in order to include details not resolved in the available structures^{14,34} such as improved models of the glycosylation. We think that these details, which are essential in questions such as recognition of the spike by the immune system or its interaction with specific receptors will not be essential in the study of the interaction of the spike with extended surfaces. In any case, developments on improved spike models should be carefully considered in future simulations of the virus interactions with materials.

The spike structure was solvated using VMD with an spherical solvation shell in order to maintain its hydrated functional state. The number of TIP3P water molecules added to solvate the glycoprotein was 60,642. We also added 23 Na⁺ counterions to neutralize the charge of the spike. The system made by the hydrated spike with counterions has a total of 228,657 atoms.

The structures of the surfaces were built as follows. The cellulose structure was built using the Cellulose builder toolkit³⁵ from a cut of the crystallographic plane (100) from cellulose I β crystal structure as in our previous work²⁷. We selected the (100) cellulose surface because it is the structurally simplest and smoothest surface that can be generated from cutting the I β cellulose crystal structure (see for example Figure 2 in Ref²⁷). In any case, our previous studies²⁷ show that the different surfaces of cellulose have similar wet-

ting properties and similar hydrogen bonding capacity. An interesting feature of the (100) cellulose surface is that it has "buried" -OH groups involved in cellulose-cellulose hydrogen bonds that can be broken to generate hydrogen bonds of cellulose with adsorbing molecules (see for example Fig.3 in Ref²⁷). The generated cellulose structure has a surface with dimensions of 26.1 nm \times 25.08 nm and a thickness of 3.18 nm (8 molecular layers) as seen in Figure 2b. The cellulose structure has 252,000 atoms and the full simulation box with the hydrated spike, Na⁺ counterions and cellulose has 480,633 atoms.

The graphite structure was build using the inorganic builder plugin of VMD⁴ by replicating the unit cell 100 times in *a*, 100 times in *b* and 3 times in *c* direction. A detail of the surface can be observed in Figure 2c. Since graphite has a hexagonal crystal structure, we used also periodic boundary conditions with the same geometry, with simulation box vectors (in nm) *a*=(12.28,-21.27,0.00), *b*=(12.28,21.27,0.00), *c*=(0.00,0.00,40.0). The graphite structure has 120,000 atoms and the full simulation box (hydrated spike, counterions and surface) contains 348,654 atoms.

We recall here that all surfaces considered in our simulations are neutral.

B. Molecular Dynamics simulations protocols

The protocol followed in all simulations includes an initial minimization, equilibration and production runs. In all simulations Newton's equations of motion were integrated with a 2 fs time step and electrostatic interactions were updated every 4 fs. All bonds between heavy atoms and hydrogen atoms were kept rigid. All simulations were performed in the NVT ensemble with a Langevin thermostat set at 298 K and a damping coefficient of 1 ps⁻¹. We employed periodic boundary conditions in all directions. Lennard-Jones interactions were computed with a cutoff of 1.2 nm and a switching function starting at 1.0 nm. Electrostatic interactions were computed using Particle Mesh Ewald (PME) algorithm using a real space cutoff set at 1.2 nm and a PME grid of 1.0 Å.

We performed three different MD simulations. First, we performed a preliminary simulation (19 ns) of the solvated spike at 298K. Employing the results of the preliminary simulation as starting configuration, we have performed MD simulations of the protein spike adsorption onto cellulose and graphite. The equilibrated spike inside a water droplet was positioned at 2 Å away from the surface, as shown in 2. The simulation trajectory was run for 83.4 ns in the case of adsorption onto cellulose and 88.5 ns in the case of graphite.

C. Analysis of results

The snapshots and movies of the simulations were made using Visual Molecular Dynamics (VMD) software⁴. The different analysis were made using VMD tools and appropriate scripts as follows.

As discussed in the main paper, for convenience in the analysis we introduce an initial adsorption stage and a the final adsorption stage. In the calculations of averaged quantities, the exact definition of these stages is as follows. We define the initial adsorption stage as the time interval between 12.55-19.44 ns for simulations of adsorption over the cellulose surface and between 11.0-21.0 ns for the case of graphite surface. Similarly, we define the final adsorption stage as the time interval between 74.5-83.4 ns for the simulation with cellulose and between 78.5-88.5 ns for the simulation with graphite. Note that this choice of time intervals is related to simplicity in data handling and the time intervals shown in Figure 4 are not exact (since the exact definitions slightly differ for each surface) but approximate for illustrative purposes.

The number of aminoacids in contact with each surface (Figure 4a) was computed considering that a contact between aminoacids and surface occurs when at least one atom of the aminoacid is found at a distance smaller than 3.5 Å from any surface atom. In order to co count the number of aminoacids at each time timestep we employed a TCL script running on VMD implementing the distance requirement described above. The distribution of residues in contact with the surfaces (Figure 6) was calculated over the initial and final adsorption stage with a similar TCL script, averaging over the intervals defined above. The 2-D contact map (Figure 6) was calculated using VMD Volmap tool for residues at distance of less than 3.5 Å from surface atoms.

The root mean squared deviation (RMSD) reported in Figure 4b was computed between each instantaneous structure and the initial structure using the RMSD trajectory tool implemented in VMD⁴.

The analysis of secondary structure as function of time in Figures 4c and 4d was made using the timeline tool in VMD, which uses the STRIDE algorithm³⁶ to calculate the fraction of different secondary structure components.

In the case of Hydrogen bonds (Figure 7) the distance and angle criteria was 3.5 Å and 30 degrees respectively.

ACKNOWLEDGMENTS

This work was supported by the Spanish Ministry of Science and Innovation through grant RTI2018-096273-B-I00 and the “Severo Ochoa” Grant SEV-2015-0496 for Centres of Excellence in R&D awarded to ICMAB. We thank the CESGA supercomputing center for computer time and technical support at the Finisterrae supercomputer. D. C. Malaspina is supported by the European Union Horizon 2020 research and innovation programme under Marie Skłodowska-Curie grant agreement No. 6655919.

Appendix A: Protein detachment by Steered Molecular Dynamics

The detachment force of the spike at cellulose and graphite surfaces adsorbed at the initial adsorption stage (Figure 3) was calculated using the Steered Molecular Dynamics technique³⁷

(SMD) as implemented in NAMD. The SMD simulations were conducted starting from the configuration obtained in the MD simulations at 21.0 ns for adsorption onto the cellulose surface and 19.44 ns for the graphite case. The spike glycoprotein was pulled from the center of mass of the residues located at less than 4nm from the surface, this roughly correspond to the RBD and NTD domains. The parameters for the SMD simulation are the same as previous simulations with the addition of a forcing to the spike (force constant 2×10^4 kcal/mol/Å²) ensuring a constant velocity of pulling that was set to 1 nm/ns, 2 nm/ns and 5 nm/ns. According to these velocities the simulation time was selected in order to obtain a separation of at least 2 nm between the spike and the surface.

As a result, in SMD we obtain force-separation curves corresponding to each pulling velocity. These forces as a function of spike-surface distance obtained in the SMD simulations were rather noisy (as usual in SMD simulations) so they were smoothed with a running average.

We should keep in mind that the obtained forces from the SMD simulations correspond to nonequilibrium processes in which the motion of the spike will experience a viscous drag (which depends on velocity) in addition to the adhesion force. This viscous resistance can be identified by noting that the force should decay to zero as the protein separates from the surface. In the SMD simulations, we observe a decay of the force with distance to an approximately constant value. This value can be taken as an approximation to the viscous resistance. Therefore, in order to remove the effect of viscous drag and extract the adhesion force, we have shifted the force versus distance curves obtained in SMD so that they decay to zero force at large spike-surface separations. The values of the estimated viscous drag depend on the spike velocity in the SMD simulations. For the simulations with the cellulose surface they were 4,933 pN, 6598 pN and 11,150 pN for SMD simulations of velocities of 1nm/ns, 2nm/ns and 5 nm/ns respectively. Similarly, the values in the case of simulations with the graphite surface for SMD simulations with velocities 1nm/ns, 2nm/ns and 5 nm/ns were 4,390 pN, 7,489 pN and 11,797 pN respectively. The force versus distance curves obtained after this process were shown in Figure 8.

For the faster detachment velocity (5nm/ns) maximum force in both surfaces is approximately similar, been ~8100 pN for cellulose surface and ~8500 pN for the graphite surface. As we reduce the detachment velocity the difference in the maximum force between graphite and cellulose becomes more important, with graphite requiring a larger force to detach the glycoprotein from the surface. At the lower detachment velocity (1 nm/ns) the maximum force for cellulose surface is ~4900 pN and ~6200 pN for the graphite surface.

REFERENCES

- ¹National Institute of Allergy and Infectious Diseases (NIAID), “<https://www.flickr.com/photos/niaid/albums/72157712914621487/>,”.
- ²A. Gardner, L. Autin, B. Barbaro, A. J. Olson, and D. S. Goodsell, “Cell-PAINT: Interactive Illustration of Dynamic Mesoscale Cellular Environments,” *IEEE Computer Graphics and Applications* **38**, 51–64 (2018).

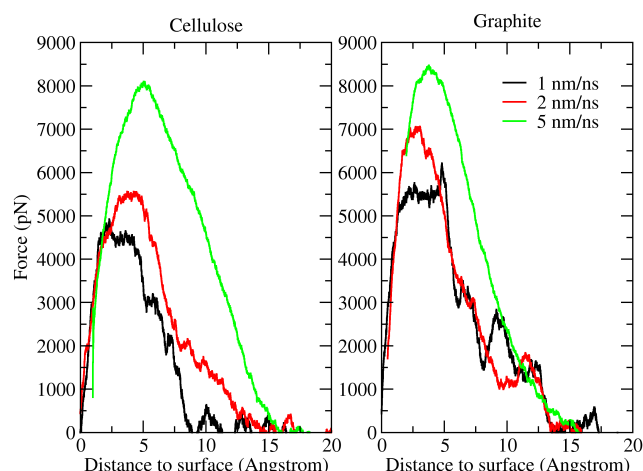


FIG. 8. Force as a function of distance, from Stereod Molecular Dynamics (SMD) results, for cellulose (left panel) and graphite (right panel) surface after the initial adsorption stage. Each line correspond to a different pulling velocity: 1 nm/ns is represented with black line, 2 nm/ns with a red line and 5 nm/ns with a green line.

- ³D. Wrapp, N. Wang, K. S. Corbett, J. A. Goldsmith, C.-L. Hsieh, O. Abiona, B. S. Graham, and J. S. McLellan, "Cryo-EM structure of the 2019-nCoV spike in the prefusion conformation," *Science* **367**, 1260–1263 (2020).
- ⁴W. Humphrey, A. Dalke, and K. Schulten, "VMD: Visual molecular dynamics," *Journal of Molecular Graphics* **14**, 33–38 (1996).
- ⁵A. E. Gorbalenya, S. C. Baker, R. S. Baric, R. J. de Groot, C. Drosten, A. A. Gulyaeva, B. L. Haagmans, C. Lauber, A. M. Leontovich, B. W. Neuman, D. Penzar, S. Perlman, L. L. Poon, D. V. Samborskiy, I. A. Sidorov, I. Sola, and J. Ziebuhr, "The species Severe acute respiratory syndrome-related coronavirus: classifying 2019-nCoV and naming it SARS-CoV-2," *Nature Microbiology* **5**, 536–544 (2020).
- ⁶World Health Organization, "WHO Timeline - COVID-19 <https://www.who.int/news-room/detail/29-06-2020-covidtimeline>," (2020).
- ⁷D. Schoeman and B. C. Fielding, "Coronavirus envelope protein: current knowledge," *Virology Journal* **16**, 69 (2019).
- ⁸R. Yan, Y. Zhang, Y. Li, L. Xia, Y. Guo, and Q. Zhou, "Structural basis for the recognition of SARS-CoV-2 by full-length human ACE2," *Science* **367**, 1444–1448 (2020).
- ⁹P. Zhou, X.-L. Yang, X.-G. Wang, B. Hu, L. Zhang, W. Zhang, H.-R. Si, Y. Zhu, B. Li, C.-L. Huang, H.-D. Chen, J. Chen, Y. Luo, H. Guo, R.-D. Jiang, M.-Q. Liu, Y. Chen, X.-R. Shen, X. Wang, X.-S. Zheng, K. Zhao, Q.-J. Chen, F. Deng, L.-L. Liu, B. Yan, F.-X. Zhan, Y.-Y. Wang, G.-F. Xiao, and Z.-L. Shi, "A pneumonia outbreak associated with a new coronavirus of probable bat origin," *Nature* **579**, 270–273 (2020).
- ¹⁰H. Berman, K. Henrick, and H. Nakamura, "Announcing the worldwide Protein Data Bank," *Nature Structural & Molecular Biology* **10**, 980–980 (2003).
- ¹¹L. Casalino, G. Palermo, A. Spinello, U. Rothlisberger, and A. Magistrato, "All-atom simulations disentangle the functional dynamics underlying gene maturation in the intron lariat spliceosome," *Proceedings of the National Academy of Sciences of the United States of America* **115**, 6584–6589 (2018).
- ¹²J. He, H. Tao, Y. Yan, S.-Y. Huang, and Y. Xiao, "Molecular Mechanism of Evolution and Human Infection with SARS-CoV-2," *Viruses* **12**, 428 (2020).
- ¹³E. S. Brielle, D. Schneidman-Duhovny, and M. Linial, "The SARS-CoV-2 exerts a distinctive strategy for interacting with the ACE2 human receptor,"

- Viruses* **12** (2020), 10.3390/v12050497.
- ¹⁴O. C. Grant, D. Montgomery, K. Ito, and R. J. Woods, "3D Models of glycosylated SARS-CoV-2 spike protein suggest challenges and opportunities for vaccine development," *bioRxiv*, 2020.04.07.030445 (2020).
- ¹⁵R. Hatada, K. Okuwaki, Y. Mochizuki, K. Fukuzawa, Y. Komeiji, Y. Okiyama, and S. Tanaka, "Fragment Molecular Orbital Based Interaction Analyses on COVID-19 Main Protease - Inhibitor N3 Complex (PDB ID:6LU7)," (2020), 10.26434/CHEMRXIV.11988120.V1.
- ¹⁶J. Wang, "Fast Identification of Possible Drug Treatment of Coronavirus Disease -19 (COVID-19) Through Computational Drug Repurposing Study," *Journal of chemical information and modeling* (2020), 10.1021/acs.jcim.0c00179.
- ¹⁷Y. Han and P. Král, "Computational Design of ACE2-Based Peptide Inhibitors of SARS-CoV-2," *ACS nano* **14**, 5143–5147 (2020).
- ¹⁸"COVID-19 Molecular Structure and Therapeutics Hub <https://covid.molssi.org/>,".
- ¹⁹P. Vasicova, I. Pavlik, M. Verani, and A. Carducci, "Issues concerning survival of viruses on surfaces," (2010).
- ²⁰L. M. Casanova, S. Jeon, W. A. Rutala, D. J. Weber, and M. D. Sobsey, "Effects of Air Temperature and Relative Humidity on Coronavirus Survival on Surfaces," *Applied and Environmental Microbiology* **76**, 2712–2717 (2010).
- ²¹J. Otter, C. Donskey, S. Yezli, S. Douthwaite, S. Goldenberg, and D. Weber, "Transmission of SARS and MERS coronaviruses and influenza virus in healthcare settings: the possible role of dry surface contamination," *Journal of Hospital Infection* **92**, 235–250 (2016).
- ²²G. Kampf, D. Todt, S. Pfaender, and E. Steinmann, "Persistence of coronaviruses on inanimate surfaces and their inactivation with biocidal agents," *Journal of Hospital Infection* **104**, 246–251 (2020).
- ²³N. van Doremalen, T. Bushmaker, D. H. Morris, M. G. Holbrook, A. Gamble, B. N. Williamson, A. Tamin, J. L. Harcourt, N. J. Thornburg, S. I. Gerber, J. O. Lloyd-Smith, E. de Wit, and V. J. Munster, "Aerosol and Surface Stability of SARS-CoV-2 as Compared with SARS-CoV-1," *New England Journal of Medicine* **382**, 1564–1567 (2020).
- ²⁴WHO, "Transmission of SARS-CoV-2: implications for infection prevention precautions <https://www.who.int/publications/i/item/modes-of-transmission-of-virus-causing-covid-19-implications-for-ipc-precaution-recommendations>," (2020).
- ²⁵H. T. Dang and V. V. Tarabara, "Virus deposition onto polyelectrolyte-coated surfaces: A study with bacteriophage MS2," *Journal of Colloid and Interface Science* **540**, 155–166 (2019).
- ²⁶A. Guo, Y. C. Shieh, and R. R. Wang, "Features of material surfaces affecting virus adhesion as determined by nanoscopic quantification," *Colloids and Surfaces A: Physicochemical and Engineering Aspects* **602**, 125109 (2020).
- ²⁷D. C. Malaspina and J. Faraudo, "Molecular insight into the wetting behavior and amphiphilic character of cellulose nanocrystals," *Advances in Colloid and Interface Science* **267**, 15–25 (2019).
- ²⁸A. Kozbial, F. Zhou, Z. Li, H. Liu, and L. Li, "Are Graphitic Surfaces Hydrophobic?" *Accounts of Chemical Research* **49**, 2765–2773 (2016).
- ²⁹R. N. Kirchdoerfer, N. Wang, J. Pallesen, D. Wrapp, H. L. Turner, C. A. Cottrell, K. S. Corbett, B. S. Graham, J. S. McLellan, and A. B. Ward, "Stabilized coronavirus spikes are resistant to conformational changes induced by receptor recognition or proteolysis," *Scientific Reports* **8**, 15701 (2018).
- ³⁰A. N. Camden, S. A. Barr, and R. J. Berry, "Simulations of peptide-graphene interactions in explicit water," *Journal of Physical Chemistry B* **117**, 10691–10697 (2013).
- ³¹D. C. Malaspina, L. Pérez-Fuentes, C. Drummond, D. Bastos-González, and J. Faraudo, "Protein-surface interactions at the nanoscale: Atomistic simulations with implicit solvent models," *Current Opinion in Colloid & Interface Science* **41**, 40–49 (2019).
- ³²J. C. Phillips, R. Braun, W. Wang, J. Gumbart, E. Tajkhorshid, E. Villa, C. Chipot, R. D. Skeel, L. Kalé, and K. Schulten, "Scalable molecular dynamics with NAMD," *Journal of Computational Chemistry* **26**, 1781–1802 (2005).
- ³³O. Guvench, S. S. Mallajosyula, E. P. Raman, E. Hatcher, K. Vanommeslaeghe, T. J. Foster, F. W. Jamison, and A. D. MacKerell, "CHARMM Additive All-Atom Force Field for Carbohydrate Derivatives and Its Utility in Polysaccharide and Carbohydrate-Protein Modeling," *Journal of Chemical*

- Theory and Computation **7**, 3162–3180 (2011).
- ³⁴L. Casalino, Z. Gaieb, A. C. Dommer, A. M. Harbison, C. A. Fogarty, E. P. Barros, B. C. Taylor, E. Fadda, and R. E. Amaro, “Shielding and Beyond: The Roles of Glycans in SARS-CoV-2 Spike Protein,” *bioRxiv*, 2020.06.11.146522 (2020).
- ³⁵T. C. F. Gomes and M. S. Skaf, “Cellulose-BUILDER: A toolkit for building crystalline structures of cellulose,” *Journal of Computational Chemistry* **33**, 1338–1346 (2012).
- ³⁶D. Frishman and P. Argos, “Knowledge-based protein secondary structure assignment,” *Proteins: Structure, Function, and Genetics* **23**, 566–579 (1995).
- ³⁷J. Hénin, G. Fiorin, C. Chipot, and M. L. Klein, “Exploring Multidimensional Free Energy Landscapes Using Time-Dependent Biases on Collective Variables,” *Journal of Chemical Theory and Computation* **6**, 35–47 (2010).